Hindawi
Geofluids
Volume 2018, Article ID 2141878, 11 pages
https://doi.org/10.1155/2018/2141878

Research Article

Field Reaction Experiments of Carbonate Minerals in Spring Waters: Natural Analogue of Geologic CO_2 Storage

Masao Sorai,[1] **Munetake Sasaki**,[1] **and Takahiro Kuribayashi**[2]

[1]*Geological Survey of Japan, National Institute of Advanced Industrial Science and Technology, Tsukuba, Ibaraki, Japan*
[2]*Department of Earth Science, Tohoku University, Sendai, Miyagi, Japan*

Correspondence should be addressed to Masao Sorai; m.sorai@aist.go.jp

Received 22 September 2017; Revised 8 January 2018; Accepted 15 January 2018; Published 12 February 2018

Academic Editor: Marco Petitta

To diminish the uncertainty of the mineral trapping rate during geologic CO_2 storage, the growth rate of carbonate minerals was measured in CO_2-containing spring waters, which can be regarded as a natural analogue of geologic CO_2 storage. The authors' approach, using nanoscale analysis of seed crystal surfaces after immersion into spring waters, enables rapid and accurate measurement of mineral reaction rates. The results show that calcite growth rates in spring waters were lower by 1–3 orders than the values given in a database of laboratory experiment results. We verified the traditional paradigm that Mg^{2+} controls carbonate reaction kinetics. An increase of the Mg/Ca ratio to around 5 by adding Mg^{2+} to spring waters markedly reduced the calcite growth rate. However, even if effects of Mg^{2+} and flow rate are considered, we were unable to explain satisfactorily the difference of the calcite growth rates between those of spring waters and laboratory experiments. Therefore, other factors might also be related to the slow growth rate in nature. The present results, including the fact such that neither dolomite nor magnesite was formed even at the high Mg/Ca ratio, are expected to provide an important constraint to overestimation of the mineral trapping rate.

1. Introduction

As a countermeasure against global warming, geologic carbon dioxide (CO_2) storage (GCS) has been proposed, whereby the CO_2 captured from a main source such as a power plant is injected artificially into a deep saline aquifer (i.e., [1]). The implementation of GCS demands elucidation not only of the CO_2 migration process, but also of the geochemical interaction in the CO_2-brine-rock system. Such an interaction proceeds along with the dissolution of CO_2 into formation waters (solubility trapping), the leaching of divalent cations from aquifer minerals into acidified waters, and carbonate mineralization from leached components and dissolved CO_2 (mineral trapping). Of these, mineral trapping is the most ideal trapping form of injected CO_2 from the viewpoint of safety. Nevertheless, it has a very long timescale: several hundred to more than several thousand years. For that reason, its magnitude and rate cannot be evaluated directly. Although we must depend on numerical simulations, such simulations include various assumptions that entail many uncertainties and numerous unknown parameters. Moreover, their output result is not necessarily reliable from the viewpoint of kinetics.

A mineral reaction rate is generally defined (e.g., [2]) as

$$\text{Rate} = kA \exp^{-E/R^*T} \Pi a_i^{n_i} f\left(\Delta G_r\right), \tag{1}$$

where k signifies the rate constant, A denotes the reactive surface area, E is the activation energy, R^* is the gas constant, T represents absolute temperature, a_i stands for the activity of species i, and n_i is the reaction order for species i. In that equation, $f(\Delta G_r)$ denotes the Gibbs free energy change of the system, which is the function of the saturation of the solution. In addition, ΔG_r is defined as (2) using activity product Q and equilibrium constant K_{eq} as

$$\Delta G_r = R^* T \ln\left(\frac{Q}{K_{\text{eq}}}\right). \tag{2}$$

Regarding (1), past numerical simulation studies have not devoted sufficient attention to $a_i^{n_i}$, except for cases in which i is a proton. This term denotes the promotional

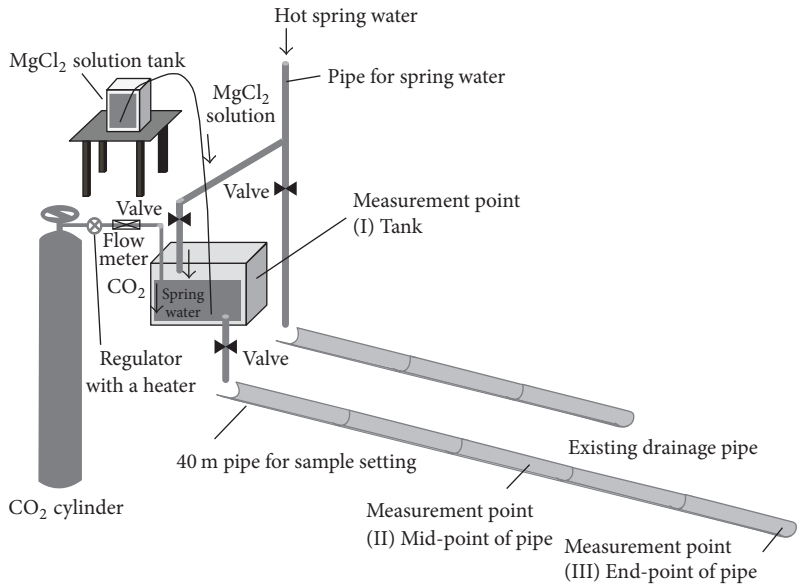

Figure 1: Schematic diagram of the field experiment system.

or inhibitory effects of reactions induced by an impurity. Actually, it is unrealistic to examine the effect of all chemical species dissolved in formation waters on each mineral. For example, however, the magnesium ion Mg^{2+} is well known to inhibit the formation of calcium carbonate ($CaCO_3$): the most important CO_2-fixing mineral [3–13]. Considering that formation waters universally contain Mg^{2+}, we should therefore incorporate such a fundamental effect into the above rate.

The initial setting of the mineral species also strongly affects the simulation result. Although the starting mineral can be set from the mineral composition of rock samples collected from the target site, the later-forming secondary mineral cannot be determined solely from the thermodynamic stability. In other words, analysis from a kinetic viewpoint requires knowledge of the reaction rate that is applicable to real environmental conditions, even for the stable phase, in addition to setting of the metastable phase as an intermediate product [14]. In this context, geochemical simulations of GCS in sandstone aquifer often assume the CO_2 fixation as mineral forms of dolomite ($Ca\text{-}Mg(CO_3)_2$) or magnesite ($MgCO_3$). However, the production of these carbonates as a primary mineral is extremely restricted in nature. As a result, no knowledge exists of whether they actually precipitate in GCS conditions.

Generally, it has been pointed out that the reaction rate in nature is much lower than that obtained from laboratory experiments because of various factors such as reaction time, surface area, surface conditions (e.g., defects and clay coatings), brine compositions, material transfer, and biologic activities [15, 16]. The alternate natural analogue study allows one to obtain qualitative knowledge of geochemical reactions over a geologic timescale according to an equilibrium theory, but it fails to estimate the actual reaction rate because the reaction process remains unknown. Instead, if the mineral sample, which is characterized in advance, is exposed to the field and is then recovered after reaction, then analysis of this sample would enable the quantitative estimation of the reaction rate in nature.

This study, conducted with the intention of improving the accuracy of geochemical simulation on GCS, measured both the saturation and impurity effects on the growth rate R of carbonate minerals, and examined the formation conditions of various carbonate minerals. As a new approach to dissipate the discrepancy between laboratory and underground conditions, we used seed crystals at the CO_2-containing spring to conduct a field reaction experiment, which can be regarded as a natural analogue of GCS.

2. Methods

2.1. Reaction System. The Utoro hot spring in Shari, Hokkaido, was selected as the experiment site. The area geology consists of Neocene rocks such as andesite, rhyolite, and andesitic and rhyolitic tuffs, sandstones, and mudstones, and Quaternary andesitic rocks belonging to the volcanoes of Shiretoko. The spring water is categorized as $Na\text{-}Cl\text{-}HCO_3$ type.

We constructed the reaction system: spring water, pumped up from the spring source, was stored in a 60 L plastic tank; then the water was drained through a 40 m long PVC pipe. The drainage rate can be controlled arbitrarily by adjusting the drains attached to each upper and lower stream of the tank. Moreover, the addition of any chemical species into the tank water allows examination of the effects of such impurities specifically beyond the chemical composition of natural spring water. We set three measurement points: the tank interior (point I), the pipe midpoint (point II), and the pipe endpoint (point III). At each point, crystal samples were immersed into spring waters. Figure 1 presents a schematic diagram of the field experiment system.

Table 1: Experimental conditions.

	Additives	Flow rate (L/min)	Maximum reaction time (h)	Remarks
Run A	—	3	21	
Run B	Gaseous CO_2	3	22	
Run C	$MgCl_2$	3	23	
Run D	—	36	1	Only calcite and aragonite
Run E	—	9	1	Only calcite and aragonite

2.2. Experimental Condition. Experiments of five kinds (Runs A–E) were performed with different additives and flow rates, as shown in Table 1. The flow rate from the tank was fixed as 3 L/min in Runs A–C. It was increased, respectively, by 12-fold and 3-fold in Runs D and E. In Run B, the CO_2 from twin liquefied CO_2 cylinders was flowed through a pressure-reduction valve and was bubbled directly into the spring water in the tank at the approximate flow rate of 20 L/min. In Run C, the highly concentrated magnesium chlorite ($MgCl_2$) solution, prepared by dissolving $MgCl_2$ reagent in the spring water, was added to the tank with a constant flow rate by a tubing pump.

We used carbonate seed crystals of four kinds: calcite, aragonite, dolomite, and magnesite. These single crystals were crushed to make blocks of a few millimeters, which were adhered on a stainless plate by resin with the plane of cleavage oriented upward. As a reference surface, a part of each cleavage plane was pressed and covered by a silicone rubber film. For shorter time experiments (i.e., 1 h), part of the surface was covered with platinum-palladium by sputtering.

The maximum times to immerse crystal samples were, respectively 21, 22, and 23 h for Runs A, B, and C. These reaction times are long enough compared to previous studies of carbonate growth (e.g., [6, 8, 11, 12]). For calcite and aragonite, three or four samples were set at all measurement points. They were taken out one-by-one after 1 and 6 h. Only point III also included the sample after 3 h. The numbers of dolomite and magnesite samples were decreased: two samples at each measurement point. They were taken out only after 6 h. For Runs D and E, only calcite and aragonite were set to points I and III and were taken out after 1 h. For sampling, the moisture adhered onto the crystal surface was removed quickly using compressed air.

2.3. Surface Analysis. We observed the surface of reacted sample using differential interference microscopy (DIM). Then we analyzed its vertical configuration using a phase-shift interferometer (Fabulous; Olympus Co.) or a laser microscope (VK-8510; Keyence Co.) [18]. To evaluate the growth rate, the difference in height level between a reference and reacted surface, Δh, was measured for the vertical cross-section profile between two points set arbitrarily on the crystal surface. The height of the reacted plane was ascertained from an average along the vertical cross-section profile.

The grown phase was identified using an imaging-plate X-ray diffractometer (R-AXIS IV++; Rigaku Corp.), where an imaging plate enables production of the diffraction pattern in a short time, even for small samples. The method is the following: the solid material formed or adhered on the seed crystal was whittled away using a needle, mixed with nail polish, rolled into a sphere of several tens of micrometers, and fixed on a 10 μm diameter needle tip. The diffraction pattern was measured by rotating the needle locked on the sample holder. This mineral identification was performed only for samples set at points I and III.

2.4. Solution Analysis. At each measurement point, the temperature (±0.1°C), pH (±0.01), and EH (±0.01 mS/cm) were monitored continuously and were recorded every 10 s using a data logger. Moreover, the spring water was collected during experiments. In this instance, the in situ measurement of electric conductivity and dissolved CO_2 concentration were done, where the concentration of dissolved CO_2 (±1 mg/l) and HCO_3 (±1 mg/l) was calculated from titration to both pH 4.8 and to pH 8.3. After bringing back the collected water, we applied ICP-AES (inductively coupled plasma-atomic emission spectroscopy) to analyze both cation and silica component, except for ion chromatography for Cl and SO_4. The analytical precision of these measurements was within 3 to 5%.

3. Results

3.1. Spring Water Compositions. Table 2 presents the chemical composition of the spring water obtained at points I–III, along with the degree of saturation with respect to each carbonate mineral, $\log \Omega$ ($\Omega = Q/K_{eq}$). The $\log \Omega$ and CO_2 fugacity (f_{CO2}) was calculated using geochemical software: The Geochemist's Workbench (Aqueous Solutions Llc). In this experiment, we expected that the $\log \Omega$ increased as the water flowed down because the CO_2 originally contained in the water would be degassed during drainage process. In fact, however, point II showed the lowest $\log \Omega$, although the highest $\log \Omega$ was found predictably at point III.

In Run B, the spring water was not actually equilibrated with CO_2 at 1 bar, and the f_{CO2} remained to be 0.37 bar. This is because the tank was not enclosed completely and also the residence time of spring waters within a tank was short.

In Table 2, the solution at point II in Run B shows a negative value of $\log \Omega_{ara}$, but indeed aragonite was grown as described herein. For this reason, presumably, the solution was supersaturated with respect to aragonite, but an error in solution analysis causes the mistaken $\log \Omega_{ara}$ value.

It is noteworthy that the Mg^{2+} concentration at point I in Run C is comparable to that in Run A despite the addition of $MgCl_2$. For this reason, the sampling point within the

Table 2: Chemical compositions of spring waters at each measurement point in three runs (mg/L).

Run	Run A			Run B			Run C		
Point	I	II	III	I	II	III	I	II	III
Temp. (°C)	54.2	49.7	45.7	53.8	47.8	41.2	50.3	41.0	33.3
pH	7.14	7.17	7.97	6.53	6.54	7.84	7.31	7.26	7.99
Na	1700	1700	1800	1800	1800	1800	1700	1700	1700
K	62	62	63	62	63	63	63	63	64
Ca	110	110	100	110	110	100	110	110	110
Mg	35	35	34	34	35	34	34	310	300
Sr	4.3	4.4	4.1	4.3	4.2	4.0	4.3	4.1	4.0
Ba	0.1	0.1	0.1	0.1	0.1	0.1	0.1	0.1	0.1
Al	<0.01	<0.01	0.01	<0.01	<0.01	<0.01	<0.01	<0.01	<0.01
Fe	0.06	0.02	0.03	0.34	0.08	0.04	0.07	0.02	0.02
Mn	0.11	0.11	0.10	0.10	0.11	0.09	0.11	0.11	0.11
Cl	2100	2100	2100	2100	2100	2100	2200	3000	3000
HCO_3	1091	1110	1075	1087	1092	1072	1132	1110	1087
SO4	320	320	310	310	320	300	320	320	310
SiO_2	34	34	34	34	34	34	34	34	34
CO_2	72	77	28	261	204	28	69	68	20
$\log \Omega_{cal}$	0.87	0.85	1.53	0.23	0.14	1.35	1.01	0.77	1.38
$\log \Omega_{ara}$	0.71	0.69	1.37	0.07	−0.02	1.19	0.85	0.61	1.21
$\log \Omega_{dol}$	2.60	2.55	3.92	1.31	1.11	3.53	2.85	3.30	4.46
$\log \Omega_{mag}$	0.27	0.20	0.88	−0.39	−0.53	0.64	0.36	0.99	1.50
f_{CO2} (bars)	0.10	0.09	0.01	0.37	0.31	0.02	0.07	0.06	0.01

Table 3: Formation phase on each seed crystal.

Run	Point	Calcite	Aragonite	Dolomite	Magnesite
Run A	I	Cal	Ara	DL	Am
	III	Cal	Ara	Cal	Cal, Ara
Run B	I	Cal	Ara, Am	DL	Am
	III	Cal	Ara	Ara	Cal, Ara
Run C	I	Cal	Ara	Cal	Cal
	III	Cal	Ara	Cal, Ara	Ara

Cal, calcite; Ara, aragonite; Am, amorphous phase; DL, below detection limit.

tank was distant from an outlet of $MgCl_2$ solution. The tank water was not necessarily well mixed. Such mixing would have caused sampling of the water for which the composition was similar to that of original water. The crystal sample was exposed to high Mg^{2+} water because it was located near an outlet from the tank. Therefore, we assumed that the Mg^{2+} concentration at point I was equal to that at point II for Run C.

3.2. Crystal Surface. Figure 2 corresponds to the DIM images at each measurement point in Runs A–C. At every measurement point in Runs A–C, crystal planes of both calcite and aragonite started to grow immediately after the start of experiments. Moreover, expansion of the hillock was readily apparent on calcite surfaces. Such a tendency was more noticeable at point III. Results also show that the amount of growth in Runs B and C was less than that in Run A. Specifically, in Run C, the growing part of calcite at point III presented the fine crystalline form.

In contrast, neither dolomite nor magnesite seed crystals grew. At point III, block or needle-like crystals, which became larger over time, were formed on dolomite and magnesite surfaces. The size of these crystals in Run C increased compared to those in Run A.

Table 3 presents results of identification obtained from X-ray diffractometry. The phases grown, respectively, on calcite and aragonite seed crystals were definitely calcite and aragonite. Similarly, we confirmed that the euhedral crystals on dolomite and magnesite seed crystals were also calcite or aragonite. Specifically, additives on dolomite seed crystals at point I were not identifiable because their amounts were too small to detect using X-ray diffractometry. Moreover, the existence of amorphous phase was suggested on magnesite seed crystal at point I in Runs A and B (and partially on aragonite in Run B). However, it is not clear that the amorphous phase in Run A actually derived from mineral reactions because of its very little amount.

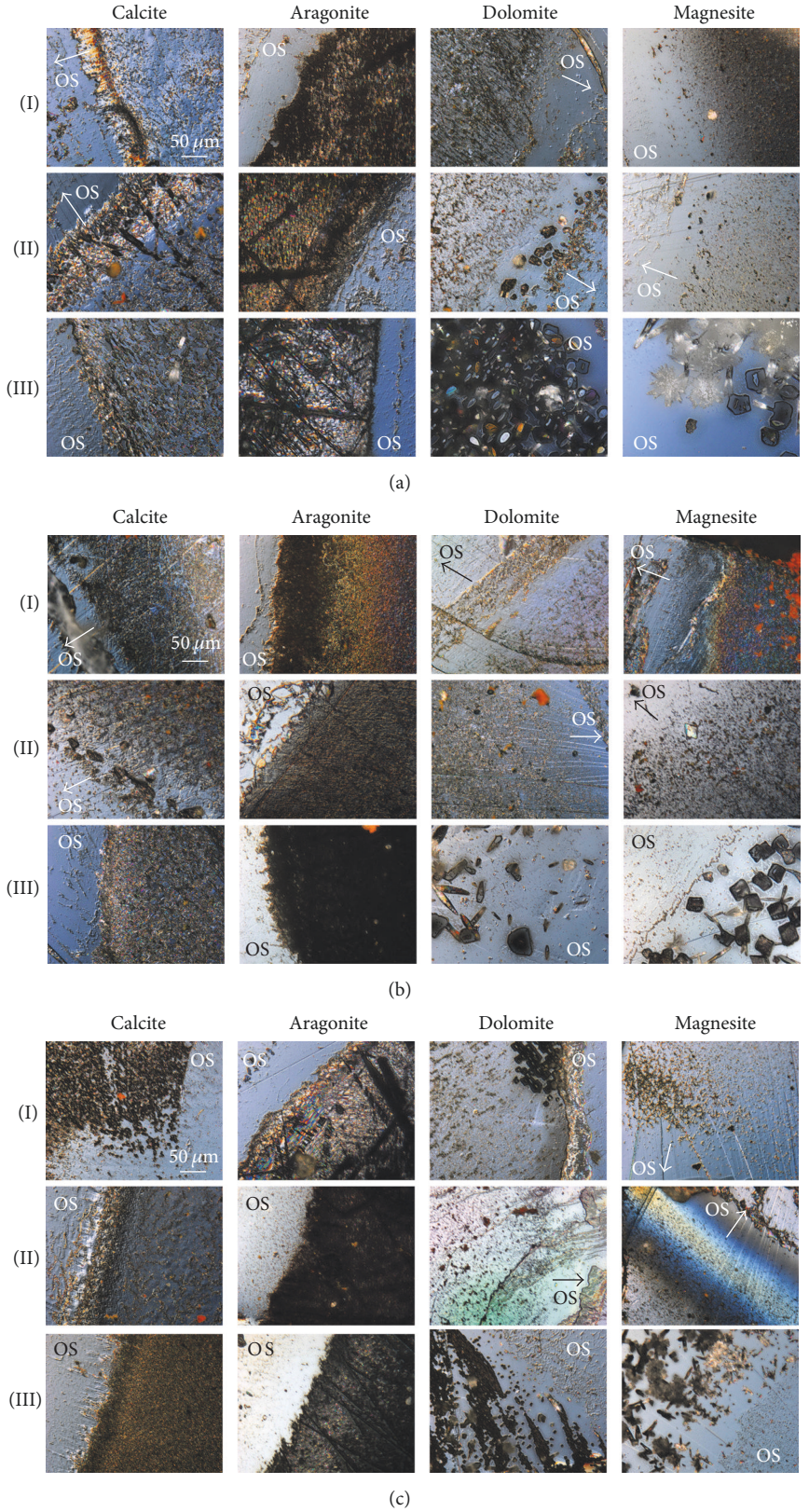

Figure 2: DIM images of sample surfaces: (a) after 21 h in Run A, (b) after 22 h in Run B, and (c) after 23 h in Run C. Part of the original surface covered by a silicone rubber film during experiments is denoted as "OS."

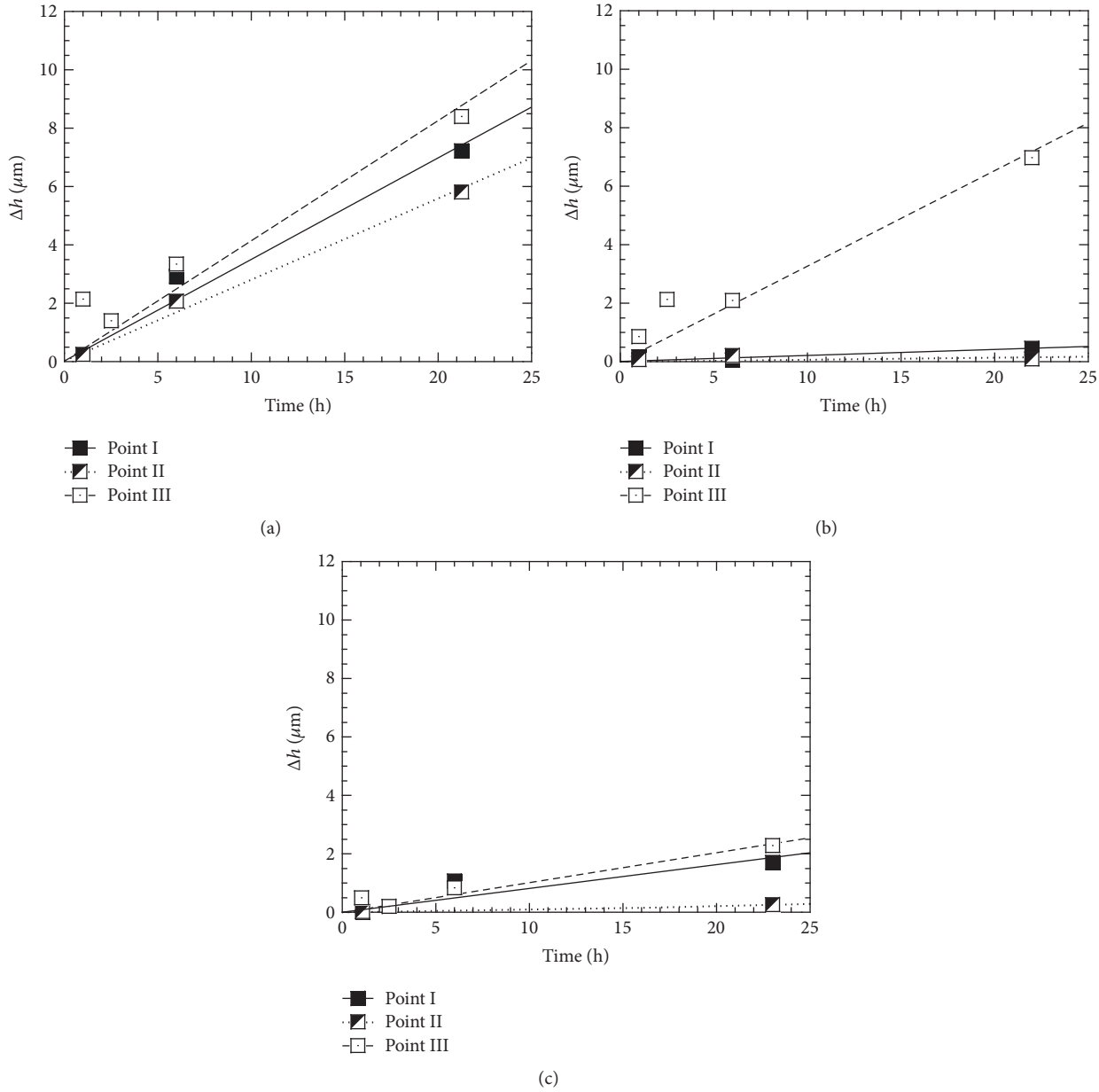

Figure 3: Time course change of Δh of calcite in each run: (a) Run A, (b) Run B, and (c) Run C. Each line corresponds to a linear approximation passing through the origin.

3.3. Growth Rate. The R was analyzed for calcite and aragonite because only these two minerals showed growth of their own surfaces. Figures 3 and 4, respectively, portray the time course change of Δh of calcite and aragonite at each measurement point in Runs A–C. We measured different crystal samples at each measurement time, which caused data dispersion. Nevertheless, both minerals increased Δh with an almost constant rate. The value of Δh at point III was the largest at all reaction times, although Δh at points I and II did not change systematically.

The comparison of each run highlighted that the calcite growth rate R_{cal} at points I and II in Run B and at all points in Run C was decreased markedly compared to the results obtained from Run A. Aragonite in Runs A and B also exhibited a similar trend to those found for calcite. However, Run C showed a different aspect: aragonite growth rate R_{ara} was reduced only at point III.

4. Discussion

4.1. R in Spring Waters

4.1.1. Saturation State Dependence of R. We calculated R by dividing the slope of linear approximation to Δh in Figures 3 and 4 by the molar volume. The saturation dependence of R for calcite and aragonite is presented, respectively, in Figure 5.

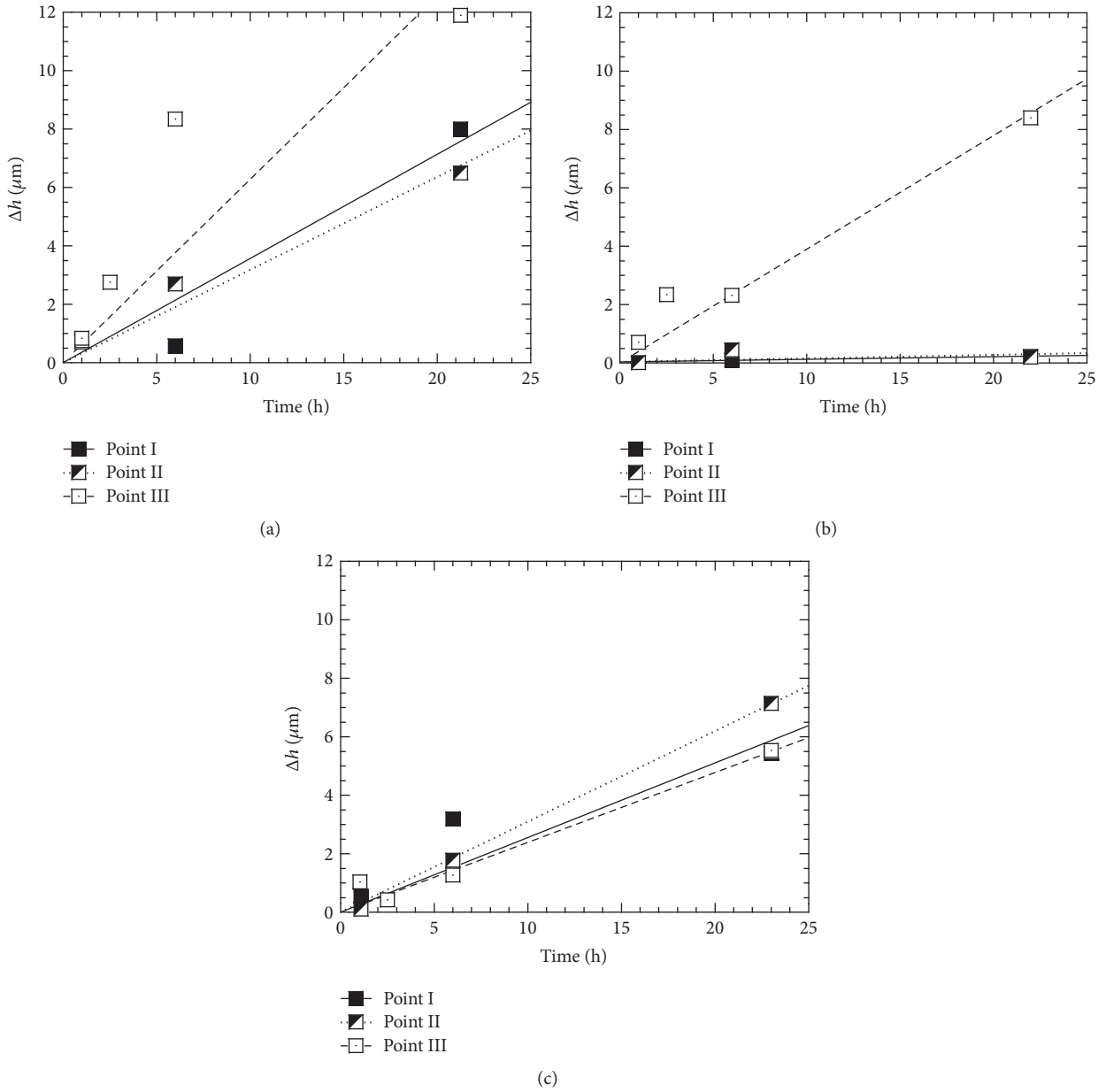

Figure 4: Time course change of Δh of aragonite in each run: (a) Run A, (b) Run B, and (c) Run C. Each line corresponds to a linear approximation passing through the origin.

In Run B, R of both minerals was decreased relative to Run A because the CO_2 injection lowered the degree of saturation at each measurement point. Such a reduction of R was noticeable at points I and II, where the initial $\log \Omega$ was low. Here, the pH change can also affect R, but the pH decrease remained at 0.6, even at point II with the highest pH reduction (Table 2). Therefore, considering the fact that the pH provides no impact to carbonates' R in the neutral range, only the degree of saturation is definitely responsible for R reduction. Regarding the effect of CO_2 injection on R, no distinct difference was found between calcite and aragonite.

In Run C, the enhanced Mg/Ca ratio, that is, ten times that of original waters, caused a significant decrease of R_{cal} at all measurement points, keeping $\log \Omega$ almost constant (Figure 5(a)). Specifically, R_{cal} at point II was decreased to just 4% of R_{cal} in Run A. This result confirms that Mg^{2+} inhibits calcite growth [5, 6, 8, 11, 12]. For aragonite, an increase of the Mg/Ca ratio provided little impact to R_{ara} (Figure 5(b)). These results are consistent with the findings reported by Berner [5] that the Mg^{2+} controls only R_{cal} and that it does not affect R_{ara}.

Here, it is noteworthy that R_{cal} in Runs A and B can be shown on a unique curve, but that R_{cal} in Run C deviates from this curve (Figure 5(a)). In other words, addition of Mg^{2+}

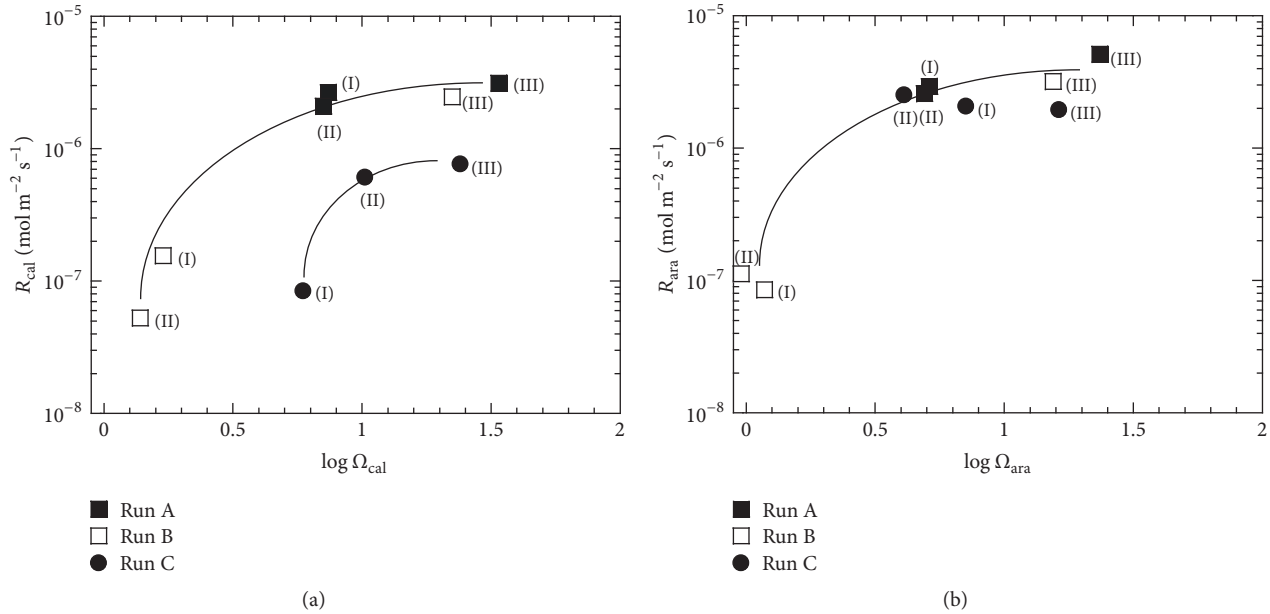

FIGURE 5: The log Ω dependence of R: (a) calcite and (b) aragonite. Roman numerals near respective dots denote measurement points. Each curve was drawn arbitrarily to clarify the trend of the relation between R and log Ω.

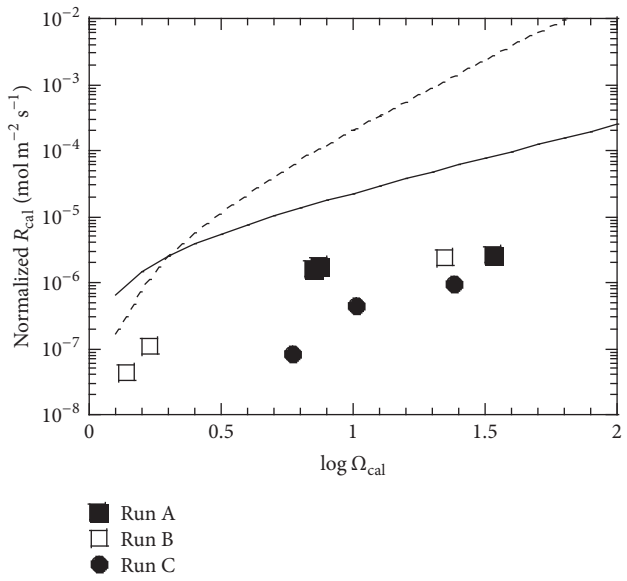

FIGURE 6: Comparison of R_{cal} between spring water and laboratory experiments.

not only changes R_{cal} but also changes the calcite growth mechanism itself.

4.1.2. Deviation of R_{cal} between Nature and Laboratory. The reaction rate database compiled by U. S. Geological Survey (USGS) was applied to compare the R found in nature and in the laboratory. The database presents the respective reaction rates of typical minerals based on many past references, particularly addressing laboratory experiments [19]. Figure 6 presents the comparison between R_{cal} found in this study and R_{cal} calculated by assuming surface-controlled and diffusion-controlled growth mechanisms. Actually, T and pH were more or less varied depending on the experimental conditions and measurement points. Therefore, the measured R was corrected to the value at 40°C and pH 7 using the functions of T (activation energy E = 23.5 kJ mol^{-1}) and pH dependence from the USGS database [19]. As described above, in fact, the pH change effect was negligible because the pH of spring waters corresponds to the neutral range.

Here, it is noteworthy that R_{cal} obtained in this study is significantly lower than the values calculated for both growth mechanisms. The trend of Runs A and B is lower by one order of magnitude with respect to the diffusion-controlled model and by 1–3 orders by magnitude depending on log Ω with respect to the surface-controlled model. Such a discrepancy can be attributed to the difference of the Mg^{2+} concentration. The spring waters indeed include 35 mg/L of Mg^{2+} (Table 2). However, it is highly unlikely that an increase of the Mg/Ca ratio from 0 to 0.5 reduced R_{cal} more than one order of magnitude [12]. Moreover, the difference of R_{cal} is enhanced with increased log Ω (Figure 6), but this trend is contrary to that of Mg^{2+} effect in Figure 5(a).

Comparison of Run A with Runs D and E revealed no distinct positive correlation between flow rate and R (Figure 7). In other words, under the present experimental condition, calcium carbonates grow according to the surface-controlled mechanism. The flow rate does not affect R. Only the calcite at point III seems likely to follow diffusion-controlled growth because R_{cal} in this point increases slightly with the flow rate. However, even R_{cal} when the flow rate is 36 L/min, which is apparently the almost maximum value, is lower by one order than the calculated result obtained using the diffusion-controlled model.

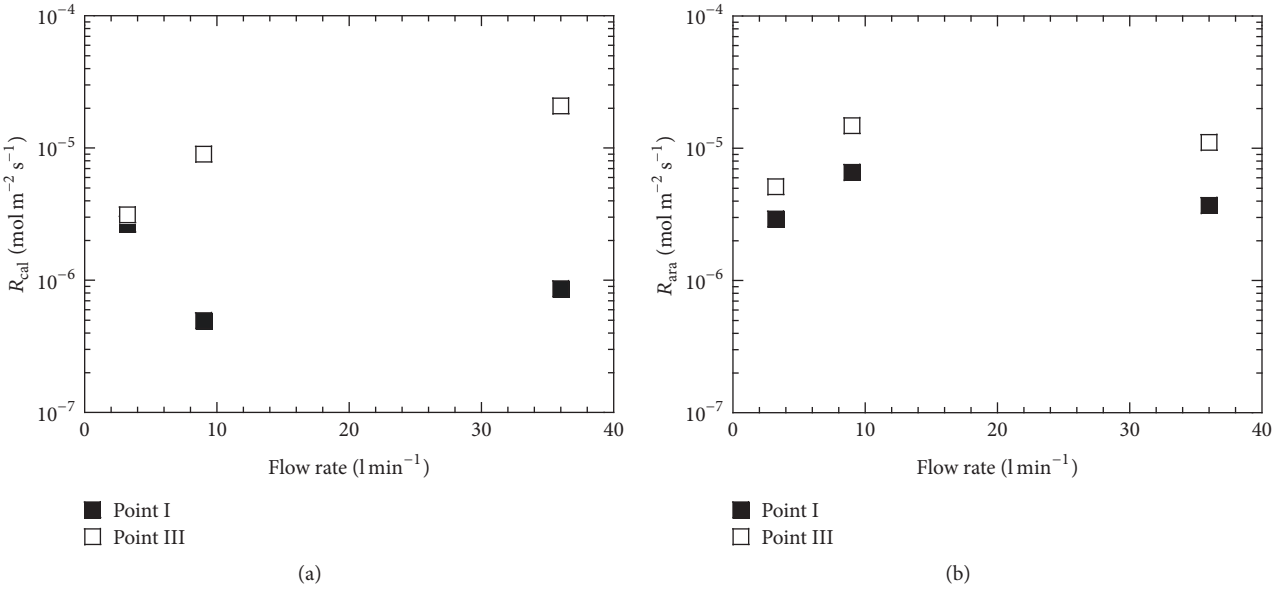

Figure 7: Flow rate dependence of R: (a) calcite and (b) aragonite.

As a result, the discrepancy of R_{cal} between the values found in nature and in the laboratory cannot be explained solely by the effects of Mg^{2+} and the flow rate. Other factors such as organic inhibitory species or biological activities might be related singly or compositely. Quantitative evaluation of each factor is beyond the scope of this work, but the result highlighted that the actual value R_{cal} can be much lower than our expectation.

4.2. Formation Phase of Carbonate Minerals. These experiments revealed that only calcite and aragonite grew in all conditions, and that neither dolomite nor magnesite showed growth of their seed crystals.

Generally, dolomite never forms in laboratory experiments under near-surface conditions (e.g., [20]). Alternatively, a high Mg/Ca ratio, high salinity, and low sulfate ion (SO_4^{2-}) concentration are required as factors for dolomite formation [17]. In contrast, Sánchez-Román et al. [21] reported that dolomite can precipitate even at surface temperature and irrespective of the presence or absence of SO_4^{2-} under a condition assisted by microbes. In either case, the present spring water indicates low SO_4^{2-} concentration. In this study, the spring water was forced to transfer within the dolomite stability field by adding Mg^{2+} artificially (Figure 8). Furthermore, seed crystals were used to overcome the barrier for nucleation. Nevertheless, dolomite did not grow, or other carbonates (i.e., calcite and aragonite) were formed on the seed crystal surface. Therefore, even if the conditions for dolomite formation, such as the Mg/Ca ratio, salinity, and SO_4^{2-} concentration, were obtained, authigenic dolomite never forms. In fact, results show that although some dolomite precipitates from seawater with high salinity under the evaporation circumstances, most dolomite is formed from calcareous sediments by alternation through diagenesis [17]. Therefore, our results support this presumption.

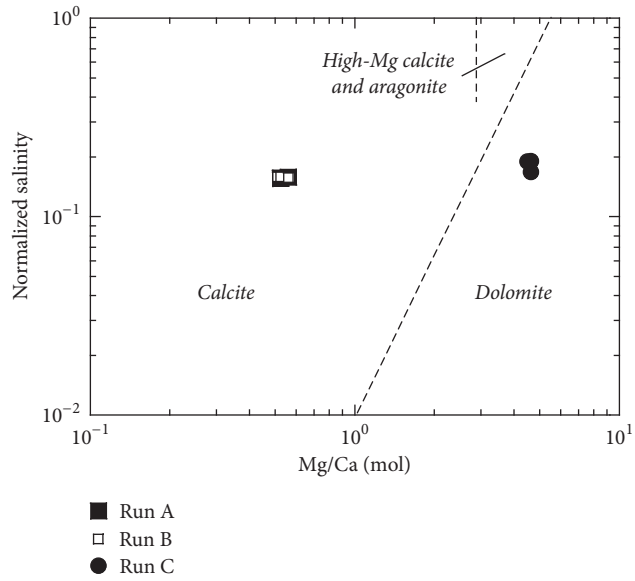

Figure 8: Stability field of calcite, aragonite, and dolomite. Phase boundaries are referred to by Matsuda [17].

Similarly, strong hydration energy of Mg^{2+} inhibits magnesite formation at low temperature [22]. Factors that might overcome this constraint include high temperature and high CO_2 pressure [23–25]. Actually, authigenic magnesite precipitation was observed at 10 MPa and 90–150°C in the presence of supercritical CO_2 [26]. In addition, Saldi et al. [27] measured the step velocity on magnesite crystal surface using atomic force microscopy under temperature conditions of 80–105°C despite a lack of high CO_2 pressure. In contrast, below 60°C, hydrated magnesium carbonate, that is, hydromagnesite ($(MgCO_3)_4{\cdot}Mg(OH)_2{\cdot}4H_2O$) or nesquehonite ($MgCO_3{\cdot}3H_2O$), has been reported to form instead

of stability phase of magnesite [28, 29]. Nevertheless, these metastable phases were not identified in this study. The reason is expected to be examined further, but it is readily apparent that Ca-carbonate is assigned priority over Mg-carbonate at least under low CO_2 pressure conditions. A small amount of amorphous phase identified at point I in Run B can be regarded as the reprecipitation of components leached from dissolving magnesite because the solutions in these cases were undersaturated with respect to magnesite, as shown in Table 2.

4.3. Implication to GCS. The present results can provide an important constraint against overestimation of the mineral trapping rate on geochemical simulations of GCS. In other words, both the magnitude of R_{cal} and its Gibbs free energy change dependence differ between those found in nature and in the laboratory.

Moreover, geochemical simulations often assume the precipitation of dolomite and magnesite. However, formation waters generally correspond to values that are out of the stability field of these carbonates (i.e., the Mg/Ca ratio of formation waters is generally not high). In addition, the formation of authigenic dolomite is at least restricted to special conditions as described above. Therefore, only calcite or aragonite is formed on GCS. Dolomite (and also magnesite in some cases) would not contribute to mineral trapping. Although the accurate judgment of magnesite formation requires further experiment under higher CO_2 pressure condition, we can conclude that the magnesite growth would be inhibited at least under low CO_2 pressure condition, such as shallow under the ground and within a reservoir far from a CO_2 plume.

If dolomite or magnesite is not precipitated, even under high Mg/Ca conditions, then Mg^{2+} remains in solution without coprecipitation, which would act as an inhibitor of R_{cal}. Consequently, R of total carbonates depends on the ratio between forming calcite and aragonite because R_{ara} is unaffected by Mg^{2+}. Hereinafter, the Mg^{2+} effect on the mineral trapping rate, including whether Mg^{2+} remains into solution or not, should be considered quantitatively and comprehensively. Misunderstanding of the formation phase of Ca-Mg carbonates is expected to affect the subsequent estimate of carbonates' R.

5. Conclusions

To diminish the uncertainty of the mineral trapping rate on GCS, R of carbonate minerals was measured at the CO_2-containing spring, which can be regarded as a natural analogue of GCS. We immersed seed crystals in flowing spring waters and analyzed nanoscale aspects of their surfaces. The authors' approach enables measurement of the reaction rates of minerals, including minerals that are not present originally, in a short time and with high accuracy.

This study specifically addressed carbonate's reaction kinetics in a Ca-Mg system. For this purpose, R and formation phase of carbonate minerals were evaluated in CO_2 or Mg^{2+} added spring water and in pure spring waters. In particular, an application of the USGS database on both T and pH dependencies highlighted the $\log \Omega$ dependence of R under the GCS conditions, in addition to the Mg^{2+} effect on R. The addition of CO_2 decreased $\log \Omega$, keeping the pH almost constant, which caused reduction of carbonate's R. This effect was enhanced in spring water with low $\log \Omega$. The present experiment did not engender the unsaturated condition with respect to carbonates, but CO_2 injection at higher pressures also allows the measurement of the dissolution rate. For the Mg^{2+} effect, an increase of the Mg/Ca ratio to around 5 decreased R_{cal} considerably. This effect also became noticeable with a decrease of $\log \Omega$. R_{cal} decreased to just 4% of the original value under conditions of the lowest $\log \Omega$. In contrast, we found no marked impact of Mg^{2+} to R_{ara}. This result is consistent with observations by Berner [5] that Mg^{2+} inhibits calcite formation and promotes aragonite precipitation, at least from a viewpoint of different Mg^{2+} effects between these minerals.

Neither dolomite nor magnesite was formed even at such a high Mg/Ca ratio. In connection with the behavior of Mg^{2+} remaining in solutions, this might affect our knowledge related to the Ca-Mg system carbonate kinetics.

However, even if all effects above and flow rate effects are considered, we cannot explain satisfactorily the difference between R_{cal} in spring waters and the values in databases of laboratory experiment results. Therefore, a problem to be examined in future studies is the verification of other factors such as organic inhibitory species and microbial activities, plus the comprehensive impacts of these factors. The present results are expected to provide important constraints on overestimation of the mineral trapping rate, as often seen in geochemical simulations of GCS.

R of carbonate minerals is important also from a viewpoint of an operation of hot spring facilities. The data are useful not only for preestimate of the formation rate of hot spring deposits (i.e., scale) within a water pipe, but also for the validation of the potential of CO_2 and Mg^{2+} as additives to suppress the scale formation.

Conflicts of Interest

The authors declare that they have no conflicts of interest.

Acknowledgments

This work was performed under management of the Ministry of Economy, Trade and Industry (METI) as part of the research and development of the CO_2 geological storage project. The authors thank Ayumu Akazawa for permission to use the spring field and also for kind cooperation with their experiments. They also thank Etsuo Kimura for both construction and operation of field experiment systems.

References

[1] IPCC, "Underground geological storage," in *IPCC Special Report on Carbon Dioxide Capture and Storage*, B. Metz, O. Davidson, H. Coninck, M. Loos, and L. Meyer, Eds., Cambridge

University Press, Underground geological storage (Coordinating lead, Cambridge University Press.

[2] A. C. Lasaga, "Theory of crystal growth and dissolution," in *Kinetic Theory in the Earth Sciences*, Princeton University Press, Princeton, 1998.

[3] J. L. Bischoff, "Kinetics of calcite nucleation: Magnesium ion inhibition and ionic strength catalysis," *Journal of Geophysical Research: Atmospheres*, vol. 73, no. 10, pp. 3315–3322, 1968.

[4] R. M. Pytkowicz, "Calcium carbonate retention in supersaturated seawater," *American Journal of Science*, vol. 273, no. 6, pp. 515–522, 1973.

[5] R. A. Berner, "The role of magnesium in the crystal growth of calcite and aragonite from sea water," *Geochimica et Cosmochimica Acta*, vol. 39, no. 4, pp. 489–IN3, 1975.

[6] M. M. Reddy and K. K. Wang, "Crystallization of calcium carbonate in the presence of metal ions. I. Inhibition by magnesium ion at pH 8.8 and 25oC.," *Journal of Crystal Growth*, vol. 50, pp. 470–480, 1980.

[7] O. Söhnel and J. W. Mullin, "Precipitation of calcium carbonate," *Journal of Crystal Growth*, vol. 60, no. 2, pp. 239–250, 1982.

[8] A. Mucci and J. W. Morse, "The incorporation of Mg2+ and Sr2+ into calcite overgrowths: influences of growth rate and solution composition," *Geochimica et Cosmochimica Acta*, vol. 47, no. 2, pp. 217–233, 1983.

[9] L. Fernández-Díaz, A. Putnis, M. Prieto, and C. V. Putnis, "The role of magnesium in the crystallization of calcite and aragonite in a porous medium," *Journal of Sedimentary Research*, vol. 66, no. 3, pp. 482–491, 1996.

[10] K. J. Davis, P. M. Dove, and J. J. De Yoreo, "The role of Mg^{2+} as an impurity in calcite growth," *Science*, vol. 290, no. 5494, pp. 1134–1137, 2000.

[11] Y. Zhang and R. A. Dawe, "Influence of Mg2+ on the kinetics of calcite precipitation and calcite crystal morphology," *Chemical Geology*, vol. 163, no. 1-4, pp. 129–138, 2000.

[12] Y.-P. Lin and P. C. Singer, "Effect of Mg2+ on the kinetics of calcite crystal growth," *Journal of Crystal Growth*, vol. 312, no. 1, pp. 136–140, 2009.

[13] J. M. Astilleros, L. Fernández-Díaz, and A. Putnis, "The role of magnesium in the growth of calcite: An AFM study," *Chemical Geology*, vol. 271, no. 1-2, pp. 52–58, 2010.

[14] I. Gaus, P. Audigane, L. André et al., "Geochemical and solute transport modelling for CO2 storage, what to expect from it?" *International Journal of Greenhouse Gas Control*, vol. 2, no. 4, pp. 605–625, 2008.

[15] A. E. Blum and L. L. Stillings, "Feldspar dissolution kinetics," in *Chemical Weathering Rates of Silicate Minerals*, A. F. White and S. L. Brantley, Eds., Reviews in Mineralogy, Mineralogical Society of America, Washington, wash, USA, 1995.

[16] A. F. White and S. L. Brantley, "The effect of time on the weathering of silicate minerals: Why do weathering rates differ in the laboratory and field?" *Chemical Geology*, vol. 202, no. 3-4, pp. 479–506, 2003.

[17] H. Matsuda, "Dolomitization and Reservoir Characteristics," *Chigaku Zasshi (Jounal of Geography)*, vol. 118, no. 2, pp. 297–308, 2009.

[18] M. Sorai, T. Ohsumi, M. Ishikawa, and K. Tsukamoto, "Feldspar dissolution rates measured using phase-shift interferometry: Implications to CO2 underground sequestration," *Applied Geochemistry*, vol. 22, no. 12, pp. 2795–2809, 2007.

[19] J. L. Palandri and Y. K. Kharaka, "A compilation of rate parameters of water-mineral interaction kinetics for application to geochemical modeling. U. S. Geological Survey," *Open File Report*, pp. 2004-1068, 2004.

[20] J. M. Gregg, D. L. Bish, S. E. Kaczmarek, and H. G. Machel, "Mineralogy, nucleation and growth of dolomite in the laboratory and sedimentary environment: A review," *Sedimentology*, 2015.

[21] M. Sánchez-Román, J. A. McKenzie, A. de Luca Rebello Wagener, M. A. Rivadeneyra, and C. Vasconcelos, "Presence of sulfate does not inhibit low-temperature dolomite precipitation," *Earth and Planetary Science Letters*, vol. 285, no. 1-2, pp. 131–139, 2009.

[22] C. L. Christ and P. B. Hostetler, "Studies in the system MgO-SiO2-CO2-H2O (II): The activity-product constant of magnesite," *American Journal of Science*, vol. 268, pp. 439–453, 1970.

[23] M. Hänchen, V. Prigiobbe, R. Baciocchi, and M. Mazzotti, "Precipitation in the Mg-carbonate system-effects of temperature and CO2 pressure," *Chemical Engineering Science*, vol. 63, no. 4, pp. 1012–1028, 2008.

[24] J. C. Deelman, "Are bacteria capable of precipitating magnesite?" *Periodico di Mineralogia*, vol. 81, no. 2, pp. 225–235, 2012.

[25] A. R. Felmy, O. Qafoku, B. W. Arey et al., "Reaction of water-saturated supercritical CO 2 with forsterite: Evidence for magnesite formation at low temperatures," *Geochimica et Cosmochimica Acta*, vol. 91, pp. 271–282, 2012.

[26] V. Prigiobbe and M. Mazzotti, "Precipitation of Mg-carbonates at elevated temperature and partial pressure of CO2," *Chemical Engineering Journal*, vol. 223, pp. 755–763, 2013.

[27] G. D. Saldi, G. Jordan, J. Schott, and E. H. Oelkers, "Magnesite growth rates as a function of temperature and saturation state," *Geochimica et Cosmochimica Acta*, vol. 73, no. 19, pp. 5646–5657, 2009.

[28] D. H. Case, F. Wang, and D. E. Giammar, "Precipitation of Magnesium Carbonates as a Function of Temperature, Solution Composition, and Presence of a Silicate Mineral Substrate," *Environmental Engineering Science*, vol. 28, no. 12, pp. 881–889, 2011.

[29] O. Qafoku, D. A. Dixon, K. M. Rosso et al., "Dynamics of Magnesite Formation at Low Temperature and High pCO2 in Aqueous Solution," *Environmental Science & Technology*, vol. 49, no. 17, pp. 10736–10744, 2015.